Received: 30 March 2021 | Revised: 4 June 2021 | Accepted: 5 June 2021

DOI: 10.1002/jrs.6180

SPECIAL ISSUE - RESEARCH ARTICLE

Journal of RAMAN SPECTROSCOPY WILEY

Multi-technique characterization of glass mosaic *tesserae* from *Villa di Teodorico* in Galeata (Italy)

Danilo Bersani[1] | **Luciana Saviane**[2] | **Alessia Morigi**[2] | **Luciana Mantovani**[3] | **Maurizio Aceto**[4] | **Laura Fornasini**[5]

[1]Dipartimento di Scienze Matematiche, Fisiche e Informatiche, Università degli Studi di Parma, Parma, Italy

[2]Dipartimento di Discipline Umanistiche, Sociali e delle Imprese Culturali, Università degli Studi di Parma, Parma, Italy

[3]Dipartimento di Scienze Chimiche, della Vita e della Sostenibilità Ambientale, Università degli Studi di Parma, Parma, Italy

[4]Dipartimento di Scienze e Innovazione Tecnologica, Università degli Studi del Piemonte Orientale, Alessandria, Italy

[5]ICCOM-CNR, Istituto di Chimica dei Composti Organometallici, Consiglio Nazionale delle Ricerche, Pisa, Italy

Correspondence
Danilo Bersani, Dipartimento di Scienze Matematiche, Fisiche e Informatiche, Università degli Studi di Parma, Parma, Italy.
Email: danilo.bersani@unipr.it

Abstract

Several glass mosaic *tesserae* were found during the archeological excavations at the *Villa di Teodorico* in Galeata (Forlì-Cesena, Emilia Romagna, Italy), dated to early sixth century AD. This work reports the results of an archeometrical investigation realized through a multi-technique approach on 16 *tesserae*. The aims of the study were the determination of the glass composition, the characterization of coloring and opacifying agents, and the definition of the technological processes involved. The glass matrix and the dispersed crystallites were characterized in detail through micro-Raman spectroscopy, field emission scanning electron microscopy with energy-dispersive X-ray spectroscopy, and X-ray powder diffraction analyses. Micro-Raman spectroscopy was proven to be very effective in the analysis of complex objects, providing information on the structure and composition of the glass and on the nature of the opacifying agents and the crystalline colorants. UV–visible–NIR diffuse reflectance spectrophotometry with optic fibers was helpful to identify the metal ions used as chromophores. The different hues were obtained by means of dispersed ions as well as crystalline compounds and metal nanoparticles. A large variety of opacifying agents was detected. Results were compared with data of contemporary mosaics within the same geographical area.

KEYWORDS

FORS, glass mosaics, micro-Raman spectroscopy, SEM-EDS, XRPD

1 | INTRODUCTION

Several materials were recovered during archeological excavations (conducted in 1942 by the Archeological Germanic Institute of Rome and in different campaigns ranging from 1998 to 2019 by University of Bologna and University of Parma) at the site of the *Villa di Teodorico* in Galeata (Forlì-Cesena, Northern Italy). This is a multilayered site because of 17 centuries of occupation, from 6th century BC to 12th century AD: a protohistoric and pre-Roman settlement, a large *villa* during Roman age, a late antique complex (early sixth to seventh century AD) known as the *Palazzo* or *Villa di Teodorico*, the Ostrogothic king who decided to build his *palatium* in this area,[1–3] and a post-Theodorician settlement related to religious context.

The most important results concern the late antique phase, when *Villa di Teodorico* was built (early sixth century AD). It was a pavilions villa with long corridors and wide open spaces. In the southeastern part, there is the thermal baths complex, completely excavated and well preserved; it is divided in a summer sector and a winter sector, with numerous rooms and an uncovered courtyard. A big octagonal room, paved with an extraordinary mosaic (Figure 1), delimited the northern border of the residence. This polygonal room and neighboring areas, also paved with mosaics, were investigated recently and belonged to the most prestigious pavilion of the Villa. Unfortunately, the southern sector of this pavilion was destroyed by landslides or erosions. The octagonal room was illuminated by big windows, covered by a dome and decorated inside with wall mosaics, as the discovery of a lot of glass mosaic *tesserae* in the collapse layers proved.

The characterization of the glass mosaic tiles is an important source of historical, technological, and archaeological information. The knowledge of the production techniques and of the employed raw materials can shed light on the importance of the Villa itself, on the evolution of the manufacturing technologies of the period, and on the possible trade routes. The task is not simple, because the mosaic tiles are mainly composed by amorphous material, where network former compounds (mostly silica) were mixed with glass modifiers and flux agents. In addition, in this kind of material, the chromatic effect is obtained in many different ways: by means of micrometric coloring crystalline materials, using nanocrystalline colloids, or by dispersing in the glassy matrix transition metal ions in very small concentrations. This means that a multi-technique analysis campaign is required in order to collect complete knowledge on the nature of all the different components, including molecular, elemental, microscopic, morphological, and chromatic information. Raman microspectroscopy is suitable as a main technique in this complex analysis, being able to obtain information on both crystalline and amorphous materials, on the bulk and on the micrometric inclusions, even embedded in the glass, without necessity of preparation of the samples. This work reports the results of an archaeometric investigation performed on different glass mosaic *tesserae* by using an analytical approach that included micro-Raman spectroscopy,[4–6] field emission scanning electron microscopy with energy-dispersive X-ray spectroscopy (SEM-EDS),[7,8] X-ray powder diffraction (XRPD),[9] UV–visible–NIR diffuse reflectance spectrophotometry with optic fibers (FORS)[10,11] and optical stereo-microscopy. The detected coloring and opacifying agents were compared with those found on contemporary and previous mosaic tiles coming from the same geographical area.

FIGURE 1 The octagonal room and its floor mosaic [Colour figure can be viewed at wileyonlinelibrary.com]

2 | MATERIALS AND METHODS

The sample set consists in 16 glass *tesserae* recovered during the archeological excavation of 2018 and 2019 in the most prestigious sector of the *Villa di Teodorico* and belonging to wall mosaics that decorated inside of the octagonal room and its vestibule[3]: five green, three red, one orange, one pink, one blue, one light blue, one black, one white, and two colorless with gold leaf (one only support, one support complete with cover glass *cartellina*) (Figure 2).

Each sample was preliminary observed using a stereo-microscope Optika, with a 10–80× magnification range, to get quickly first morphological information.

The crystalline phases were identified by means of micro-Raman analysis. Nonpolarized Raman spectra were recorded at 632.8 nm (He–Ne laser) and at 473.1 nm (Nd:YAG laser) in a nearly backscattering geometry with a Horiba LabRAM microspectrometer equipped with an integrated Olympus BX40 microscope. The spectral resolution was about 2 cm^{-1}. The power on the sample was kept under 10 mW using neutral density filters. A 50× ultra long working distance objective was used to collect the Raman signal.

Textural observations and chemical analyses on glass *tesserae* were performed using a JEOL 6400 scanning electron microscope (SEM), equipped with an Oxford energy dispersion system (EDS) microprobe. The operating conditions were accelerating voltage 20 kV and 1.2 mA current, ~1 μm beam diameter, and a counting time of 75 s.

The XRPD patterns were collected from glass tesserae R1, R2, R3, and O1 in order to determine the crystalline

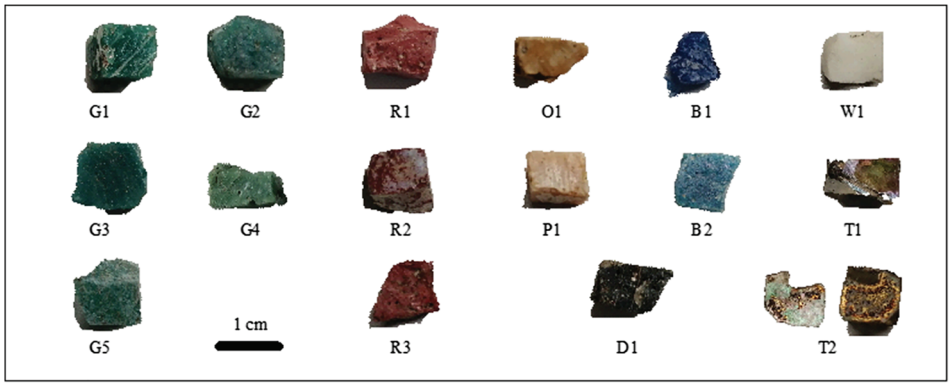

FIGURE 2 The mosaic *tesserae* investigated [Colour figure can be viewed at wileyonlinelibrary.com]

phases within the glassy matrix. The analyses were carried out on few milligrams of sample powder using a Bruker D2 Phaser diffractometer, with Cu Kα (λ = 1.54178 Å) radiation, 30 kV and 10 mA, Ni filtered, 2θ between 5 and 70°, steps of 0.02°, and a sampling time of 1 s.

FORS was useful to identify and confirm the colorants of glass *tesserae*. FORS analyses were performed with an Avantes (Apeldoorn, The Netherlands), AvaSpec-ULS2048XL-USB2 model spectrophotometer and an AvaLight-DH-S-BAL balanced deuterium—halogen light source; the detector and the light source were connected to an FCR-7UV200-2-1,5x100 probe by means of fiber-optic cables. The spot size on the sample was 2 mm.

3 | RESULTS AND DISCUSSION

3.1 | Glassy matrix

The chemical data of glassy matrix of mosaic tesserae are given in Table 1 and Figure 3. The major elements are expressed in oxides.

All glass mosaic tesserae analyzed show a composition typical of soda-lime-silica glass, with SiO_2 levels ranging from 45.4 to 80.4 wt%, Na_2O from 0.2 to 12.5 wt %, CaO from 5.7 to 13.9 wt%, and K_2O from 0.2 to 1.4 wt%.

The low concentrations of MgO and K_2O, below 1.5 wt%, suggest that probably the samples were produced using natron as flux (Figure 3a,b). The high amount of Cl (>1 wt%) and SO_3 values from 0.1 to 0.5 wt % are related to natron, which may contain NaCl and Na_2SO_4 as contaminants.[8]

The CaO (from 5.7 to 13.9 wt%) and Al_2O_3 (from 1.6 to 11.9 wt%) amounts are sometimes high (Figure 3c). This fact should be considered as intentional, because so strong levels of unwanted contamination are unlikely in those high-quality mosaic *tesserae*.

The red tesserae (R1, R2, R3), the majority of green samples (G1, G3, G4), and O1 exhibit high levels in terms of lead (PbO > 5 wt%). An important use of lead was reported in these colors[12] maybe to intensify their brightness, whereas very high lead (PbO > 20 wt%) is specifically used to produce orange *tesserae*.[12]

Manganese and antimony were usually used as decolorizing cations.[13] In fact, T1 and T2 are decolorized by the addition of MnO_2, but the support of T1 and the *cartellina* of T2 are characterized by heterogeneous glasses: In T1, some areas are richer in iron, lead, and titanium and in particular in manganese but very poor in sodium, whereas *cartellina* of T2 is formed by areas with higher values of manganese, iron, and sodium and areas with higher levels of aluminum but very low levels of manganese, iron, and sodium. These data suggest manufacturing issues for the last tesserae, such as incomplete dissolution or mixing of the raw materials.

The Raman spectra recorded on the samples, in relation to models and plots in literature,[14,15] reveal several technological information. Following the simple method for the Raman analysis of historical glasses proposed by Colomban et al.,[15] we focus our attention on the two main bands of silica glasses: the one related to Si–O–Si bending (centered at about 500 cm^{-1}) and the band attributed to Si–O stretching (at about 1000 cm^{-1}). Table 2 contains the values of Raman parameters extracted from one representative spectrum per sample: the position of the maxima δ_{max} of the bending band and the position of the maximum ν_{max} of the Si–O stretching band, together with the polymerization index I_p obtained as ratio between the intensities of the two bands (I_{500}/I_{1000}).[4,16,17] In the table, only the reliable values, extracted from the samples with the cleanest spectra, with suitable S/N ratio and low fluorescence, are reported (samples B1, B2, D1, G1, G3, and G4).

Our spectra show a position of ν_{max} ranging from 1086 to 1094 cm^{-1} and a position of δ_{max} Si–O from 560 to 590 cm^{-1}, which are compatible with values of a soda-lime-silicate glass. The values of the

TABLE 1 EDS data of the glassy matrix of mosaic tesserae

Sample	Color	SiO_2	Al_2O_3	MnO	MgO	CaO	Na_2O	K_2O	PbO	Fe_2O_3	CuO	SnO_2	Cl	SO_3	Sb_2O_3	P_2O_5	ZnO	TiO_2
B1	Blue	73.8	1.7	0.1	0.2	9.6	8.1	0.6	n.d.	2.1	n.d.	n.d.	1.2	0.2	3	n.d.	n.d.	n.d.
		1.3	0.2	0.01	0.01	0.3	1.9	0.01		0.9			0.5	0.1	0.1			
B2	Light blue	80.4	4.5	n.d.	0.5	9.1	0.8	1	n.d.	1.4	2.4	n.d.	1.3	n.d.	n.d.	n.d.	n.d.	n.d.
		1.7	0.3		0.01	0.4	0.8	0.01		0.4	0.01		0.4					
D1	Black	57.8	2.1	3.4	0.7	13.9	8.3	0.7	n.d.	12.7	n.d.	n.d.	0.9	n.d.	n.d.	n.d.	n.d.	n.d.
		2.5	0.01	0.01	0.2	0.7	0.2	0.02		1.3			0.5					
G1	Green	65.7	1.9	0.3	0.5	9.1	9.8	0.4	9.3	0.5	1.4	n.d.	1.3	3	n.d.	n.d.	n.d.	n.d.
		1.1	0.1	0.05		1.1	0.1	0.2	0.1	0.6	0.1		0.6	1.5				
G2	Green	70.8	2.5	0.4	0.7	9.2	12.5	0.7	0.2	0.4	0.7	n.d.	1.1	3	n.d.	n.d.	n.d.	n.d.
		4.2	0.5	0.05	0.07	1.3	0.6	0.06	0.1	0.1	0.1		0.6	2.3				
G3	Aqua green	54.8	4	0.3	0.8	13.7	4.8	1.4	11	3.3	4.1	5.3	1.1	n.d.	n.d.	n.d.	n.d.	n.d.
		0.8	0.04	0.05	0.09	1.8	0.1	0.2	0.01	0.06	0.1	0.01	0.4					
G4	Opaque green	64.2	1.9	1.2	0.5	8.9	10	0.6	10.8	0.9	1.6	1.5	1	n.d.	n.d.	n.d.	n.d.	n.d.
		0.9	0.08	0.02	0.1	0.01	5.4	0.4	0.03	0.05	0.5	0.05	0.1					
G5	Transparent green	71.2	2.5	0.4	0.7	9.8	12.4	0.6	n.d.	0.5	0.6	n.d.	1.2	n.d.	n.d.	n.d.	n.d.	n.d.
		1.0	0.3	0.01	0.09	0.8	0.6	0.7		0.1	0.6		0.1					
O1	Orange	45.4	2	n.d.	1.1	6	7.1	1.1	20.9	5.6	7.2	n.d.	0.5	n.d.	n.d.	n.d.	2.8	0.3
		7.2	0.5		0.05	0.9	0.1	0.9	1.5	0.5	0.1		0.5				0.09	0.06
P1	Pink	69.6	1.6	n.d.	0.6	9.4	10.7	0.9	2.8	1.4	n.d.	n.d.	1.3	n.d.	1.6	n.d.	n.d.	n.d.
		0.2	0.1		0.1	1.8	0.2	0.8	0.3	0.07			0.2		0.05			
R1	Red	64	2.3	1	1.2	8.4	11.7	1	5.2	2.3	1.5	n.d.	1	n.d.	n.d.	n.d.	0.7	n.d.
		1.4	0.1	0.002	0.1	2.4	0.1	0.05	0.1	0.1	0.06		0.5				0.1	
R2	Red	58	2.3	0.9	1	6.7	9.8	0.5	7	2.2	9.8	n.d.	0.8	n.d.	n.d.	n.d.	1	n.d.
		1.3	0.6	0.03	0.001	1.5	1.2	0.6	0.06	0.6	1.4		0.02				0.9	
R3	Red	60.1	2.1	1.7	0.7	13.7	7.8	1	5.2	3	3.6	n.d.	1.3	n.d.	n.d.	n.d.	n.d.	n.d.
		1.9	0.8	0.1	0.03	0.8	1.8	0.04	0.4	0.05	1.5		0.9					
T1	Colorless (support)	60.3	8.7	12.3	0.6	7	0.2	0.2	1.4	8	n.d.	n.d.	n.d.	n.d.	n.d.	0.4	n.d.	1
		2.1	0.02	0.03	0.6	0.3	0.6	0.5	0.5	0.1						0.1		0.02
T2	Colorless (support)	69.9	1.7	3.1	0.6	11.9	9.8	0.7	n.d.	1.1	n.d.	n.d.	0.8	0.4	n.d.	n.d.	n.d.	n.d.
		2.5	0.04	0.04	0.04	0.5	0.2	0.1		0.2			0.07	0.3				

TABLE 1 (Continued)

Sample	Color	SiO_2	Al_2O_3	MnO	MgO	CaO	Na_2O	K_2O	PbO	Fe_2O_3	CuO	SnO_2	Cl	SO_3	Sb_2O_3	P_2O_5	ZnO	TiO_2
T2	Colorless (*cartellina*)	79.4	7.5	1.1	0.4	9.1	4.7	0.4	n.d.	0.8	n.d.	n.d.	0.5	0.3	n.d.	n.d.	n.d.	n.d.
		5.3	0.05	0.07	0.09	0.4	0.6	0.2		0.3			0.3	0.2				
W1	White	77.6	11.9	0.1	0.7	5.7	0.4	0.5	n.d.	n.d.	n.d.	n.d.	0.2	0.5	2.5	n.d.	n.d.	n.d.
		9.7	0.5	0.06	0.02	0.06	0.01	0.1					0.1	0.1	0.09			

Notes: Data are expressed as weight percent (wt%). Standard deviations on the mean value are reported.
Abbreviation: n.d., not detected.

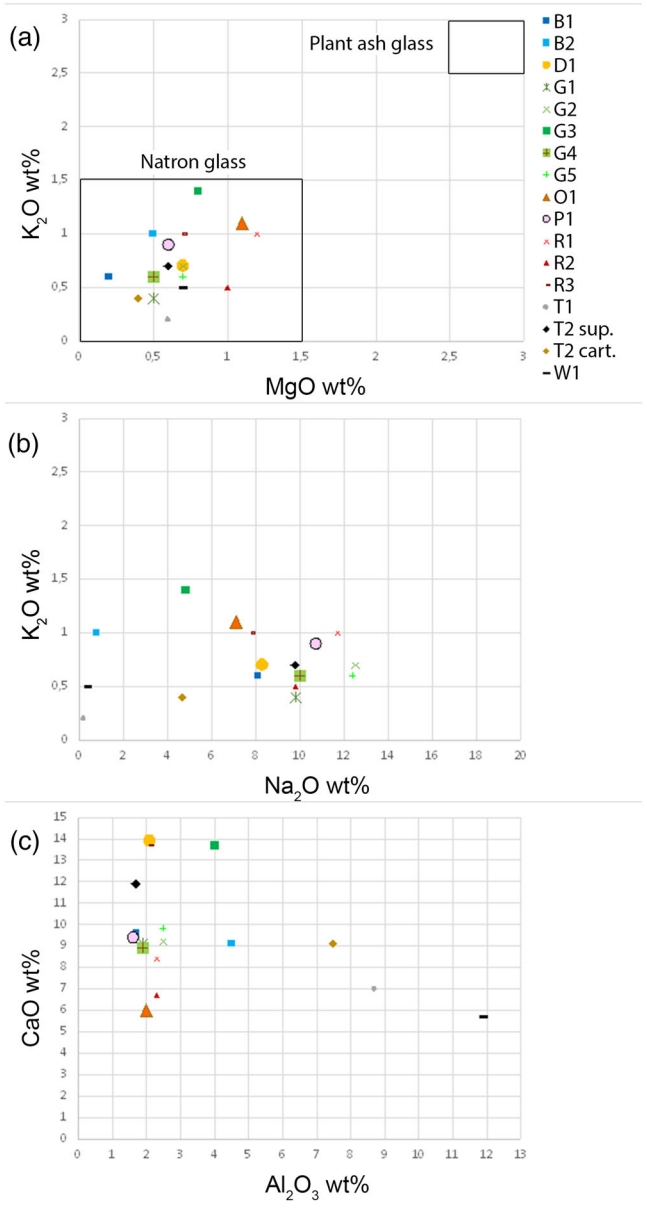

FIGURE 3 Chemical composition of the *tesserae*: (a) binary plot MgO versus K_2O; (b) binary plot Na_2O versus K_2O; (c) binary plot Al_2O_3 versus CaO [Colour figure can be viewed at wileyonlinelibrary.com]

TABLE 2 Raman parameters extracted from the spectra of B1, B2, D1, G1, G3, and G4

Sample	I_p	δ_{max} Si–O	ν_{max} Si–O
B1	1.04	560	1094
B2	1.06	560	1094
D1	0.98	590	1087
G1	1.05	570	1094
G3	0.81	580	1086
G4	0.81	580	1086

Note: Wavenumber positions in cm^{-1}.

polymerization index I_p vary in the range 0.81–1.06, typical of most Roman alkaline glasses ($0.8 < I_p > 1.1$),[15] confirming the results of SEM-EDS. Moreover, the strong correlation between the polymerization index and the wavenumber maxima of the Si–O bending and stretching allows to confirm that the analyzed *tessera*e belong to family of $Na_2O + K_2O + CaO$ glasses, as the comparison between Raman spectra and literature suggests.[4,17] Finally, because of the empirical relationship between I_p and the firing temperature, we can suppose $T_f = \sim 1000°C$ for $I_p \sim 1$, which corresponds to most ancient glasses.[15]

3.2 | Coloring and opacifying agents

The colors of tiles are blue, light blue, green, red, orange, pink, white, and black. Opacification and, in some case, coloration are obtained by tiny (nano- to micrometric) crystalline phases embedded in the glassy matrix, identified by micro-Raman spectroscopy and, for some tesserae, XRPD. Many colors were produced by transition metal ions dispersed in the glassy matrix, requiring the help of SEM-EDS and FORS for their correct identification. Table 3 provides at a glance a picture of colorants and opacifiers found; some opacifiers were acting also as coloring agents.

The red color of R1, R2, and R3 is due to metallic copper Cu^0, present as suspension of submicrometer colloidal particles, as FORS (inflection point between 590 and 595 nm)[11] and XRPD demonstrated (Figure 4a,b). Furthermore, SEM-EDS proved that copper levels of R2 (CuO 9.8 wt%) are higher than R1 (CuO 1.5 wt%) and R3 (CuO 3.6 wt%). The color of R1 and R3, where copper values are lower, was obtained probably by the combined use of copper (CuO 1.5 and 3.6 wt%, respectively) and iron (Fe_2O_3 2.3 and 3 wt%, respectively) in a lead-rich matrix (PbO 5.2 wt% in both samples).[4] Metallic copper operates as colorant but also as opacifying agent together with cassiterite (SnO_2), co-opacifier identified by XRPD (Figure 4b), SEM-EDS, and micro-Raman spectroscopy. In fact, backscattered electron (BSE) images show an uniform distribution of aggregates of crystals that are mostly composed by tin (Figure 4c,d) and whose Raman spectrum is characterized by the typical peaks of cassiterite (the main peaks are highlighted in bold type) at 475, **634**, and 776 cm^{-1} (Figure 4e).

Starting from fourth century AD, antimony-based crystalline phases (calcium and lead antimonate) have been progressively substituted by tin-based phases,[12] maybe because of either the interruption in the supply of antimony or the beginning of closer relations between the Roman Empire and India.[18–20] Nevertheless, lead antimonate was again extensively used from 15th century to achieve an opaque yellow color in glasses and glazed ceramics and as a pigment for painting.[21] Tin-based phases are used as colorants and opacifiers in white glasses but only as opacifiers in glasses colored by metallic oxides (like copper or cobalt).

The XRPD pattern of R2 presents also three peaks (the main at about 29° 2θ), which are compatible with $PbCu_2O_2$ (Figure 4b): The attribution is not completely sure, and it could be due to contaminants in some copper oxides.

TABLE 3 Coloring and opacifying agents for all differently colored mosaic *tesserae* (some compounds acting as both colorants and opacifiers are in the column of the main role)

Sample	Color	Coloring agents	Opacifying agents
B1	Blue	Co^{2+}	$CaSb_2O_6 + CaSb_2O_7$
B2	Light blue	$Cu^{2+} + Fe^{3+}$	$Ca_3(PO_4)_2$
D1	Black	$Mn^{3+} + Fe^{3+}$	
G1	Green	Cu^{2+}	$PbSn_{1-x}Si_xO_3 + SnO_2$
G2	Green	Cu^{2+}	$SnO_2 + Ca_3(PO_4)_2$
G3	Aqua green	Cu^{2+}	$PbSn_1{-}_xSi_xO_3 + SnO_2$
G4	Opaque green	Cu^{2+}	$PbSn_1{-}_xSi_xO_3 + SnO_2$
G5	Transparent green	$Cu^{2+} + Fe^{3+}$	$SnO_2 + Ca_3(PO_4)_2$
O1	Orange	Cu_2O	SnO_2
P1	Pink	$Mn^{3+} + Fe^{3+}$	$Pb_2Sb_2O_7$
R1	Red	Cu^0	SnO_2
R2	Red	Cu^0	SnO_2
R3	Red	Cu^0	SnO_2
W1	White		$CaSb_2O_6 + CaSb_2O_7$

Note: Some compounds acting as both colorants and opacifiers are in the column of the main role.

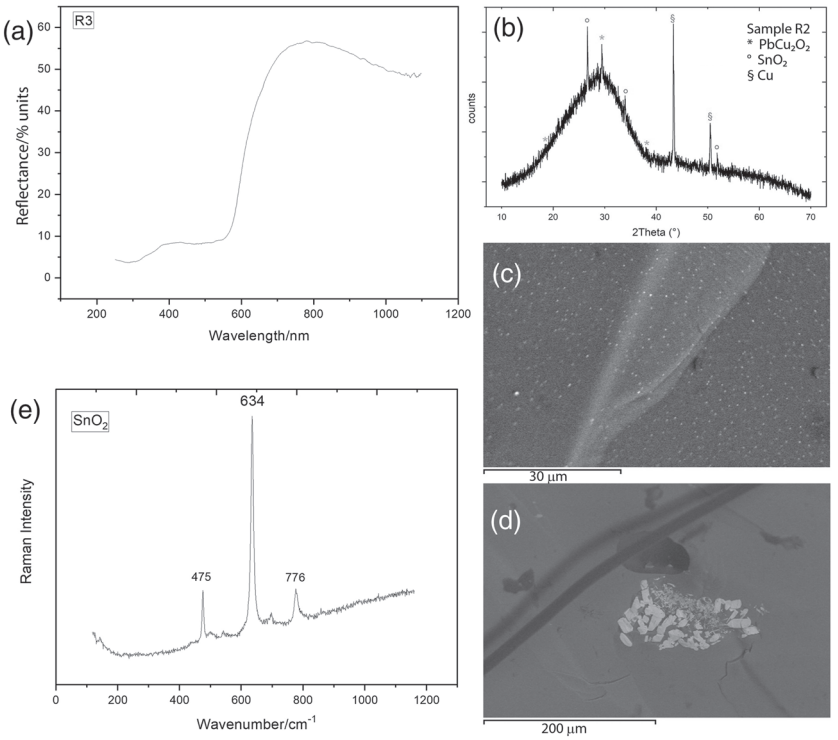

FIGURE 4 (a) FORS spectrum of R3; (b) XRPD pattern of R2; (c) BSE image of crystals of cassiterite in R2; (d) BSE image of crystals of cassiterite in R3; (e) Raman spectrum of cassiterite in R3

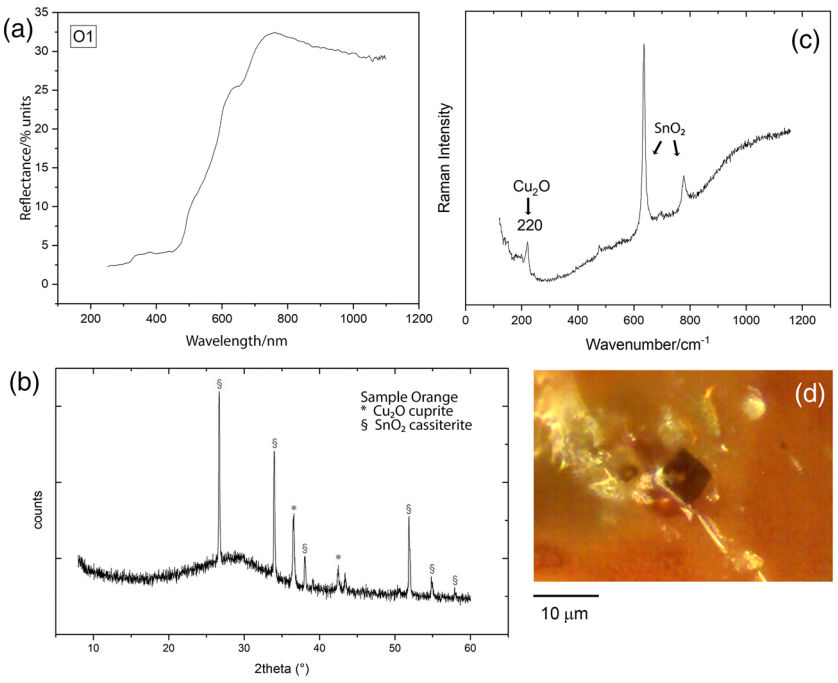

FIGURE 5 Analyses of *tessera* O1. (a) FORS spectrum; (b) XRPD pattern of O1; (c) Raman spectrum of a crystalline inclusion of Cu_2O and SnO_2; (d) microscope image of a crystalline inclusion of Cu_2O [Colour figure can be viewed at wileyonlinelibrary.com]

In the orange tile O1, FORS analyses (Figure 5a), XRPD (Figure 5b), and mainly micro-Raman spectroscopy (Figure 5c) identified cuprite (Cu_2O),[11] which acts as colorant and co-opacifier together with cassiterite (SnO_2).[18] FORS spectrum shows points of flex at 490/595/685 nm, ascribable to cuprite (Figure 5a). The Raman spectrum[4,5,11] of crystalline inclusions (Figure 5d) shows the vibrational features of cuprite with the main peak at **220** cm^{-1}, in addition to characteristic peaks of cassiterite (Figure 5c). The formation of Cu_2O needs reducing atmosphere in the furnace and high content of copper and lead,[5,18] as it is demonstrated by SEM-EDS.

Pink hue of P1 was obtained through manganese in combination with iron: FORS technique identified Mn^{3+} as colorant (minima at 380/490 nm)[10] (Figure 6a), not

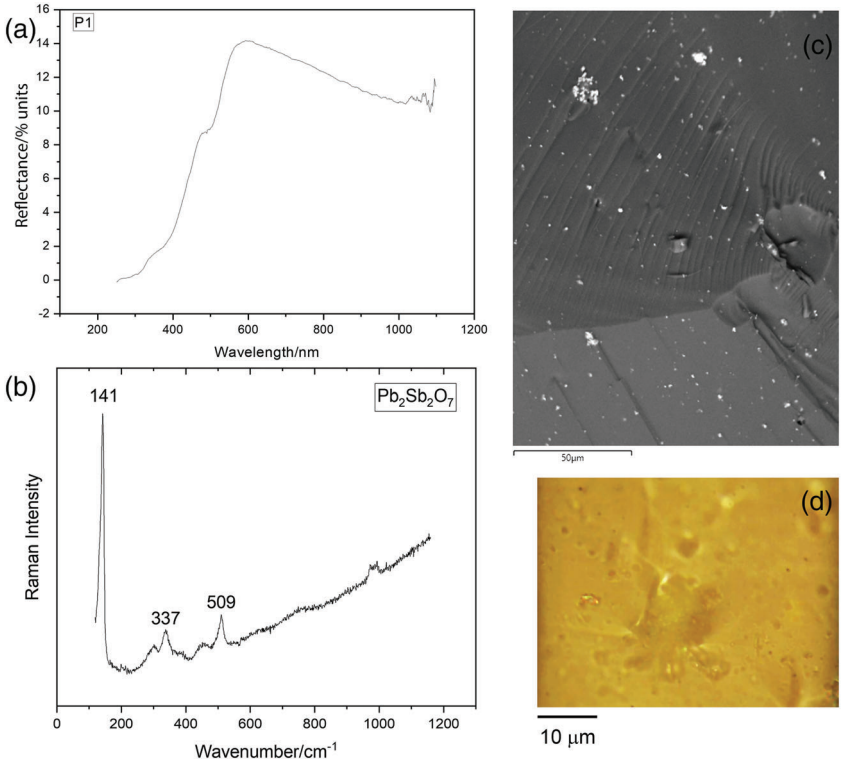

FIGURE 6 Analyses of *tessera* P1. (a) FORS spectrum; (b) Raman spectrum of a $Pb_2Sb_2O_7$ inclusion; (c) BSE image of $Pb_2Sb_2O_7$ crystals; (d) microscope image of a $Pb_2Sb_2O_7$ inclusion [Colour figure can be viewed at wileyonlinelibrary.com]

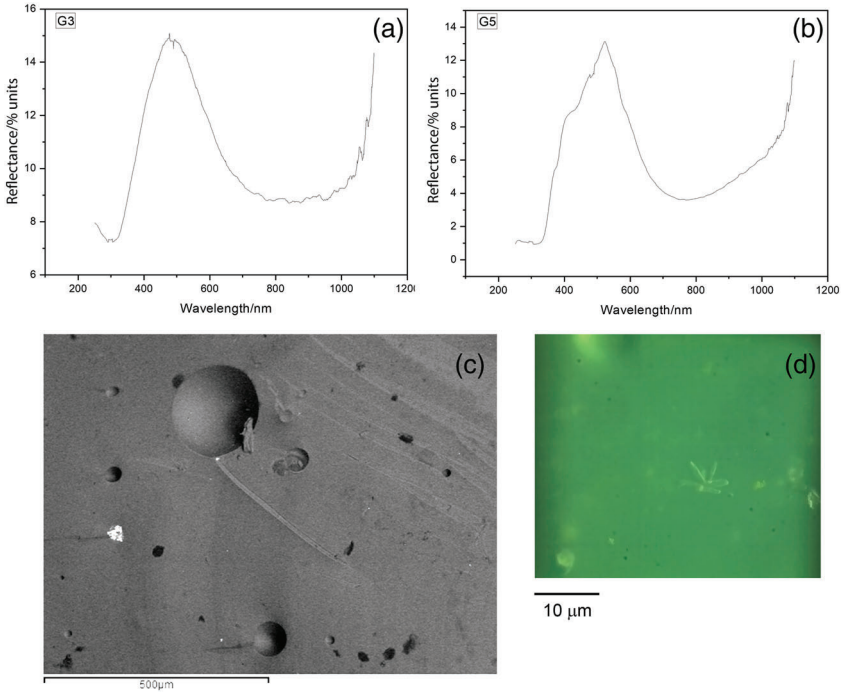

FIGURE 7 (a) FORS spectrum of G3; (b) FORS spectrum of G5; (c) BSE image of SnO_2 crystals in G5; (d) microscope image of a SnO_2 star in G3 [Colour figure can be viewed at wileyonlinelibrary.com]

detected by SEM-EDS likely because its concentration is very low. Micro-Raman spectroscopy detected hematite. This iron oxide, however, was common as coloring agent only starting from Islamic and Venetian times[4]; hence, in this case, the presence of hematite could be accidental. Bindheimite ($Pb_2Sb_2O_7$), also known as "antique yellow", was used as coloring and opacifying agent, even if it is more common in green and yellow glass *tesserae* as both opacifier and colorant.[19,22] Micro-Raman measurements carried out on yellowish inclusions (Figure 6d) allowed to recognize them as lead antimonate ($Pb_2Sb_2O_7$) crystals with peaks at **141**, 337, and 509 cm^{-1} (Figure 6b). SEM-

EDS analyses confirmed that the crystalline phases dispersed are mainly made of lead and antimony (Figure 6c).

In green *tesserae*, FORS data emphasize use of copper Cu^{2+} as chromophore (minima between 750 and 830 nm) (Figure 7a) and show some weak absorption structures of iron Fe^{3+} in G5 (bands in 375/430 nm) (Figure 7b), whereas EDS analyses show copper and iron in all samples. Cassiterite (Figure 7d) is used as opacifier and was identified by SEM-EDS (Figure 7c) and micro-Raman spectroscopy. BSE images of G1, G3, and G4 show a nonuniform microstructure (Figure 8a). In these *tesserae*, in addition to SnO_2, lead–tin yellow type II ($PbSn_{1-x}Si_xO_3$) was used as coloring and opacifying as shown by its characteristic Raman peaks at **139**, 332, and 450 cm^{-1} (Figure 8b). The presence of $PbSn_{1-x}Si_xO_3$ crystals seem to suggest a firing temperature below 1000°C, because at higher furnace temperatures, they begin to decompose.[18] Lead–tin oxides were employed for opaque yellow and green glasses in Eastern Mediterranean between the fifth and the ninth century AD and in Italy between the 6th and the 16th century AD, especially during Late Antiquity.[18]

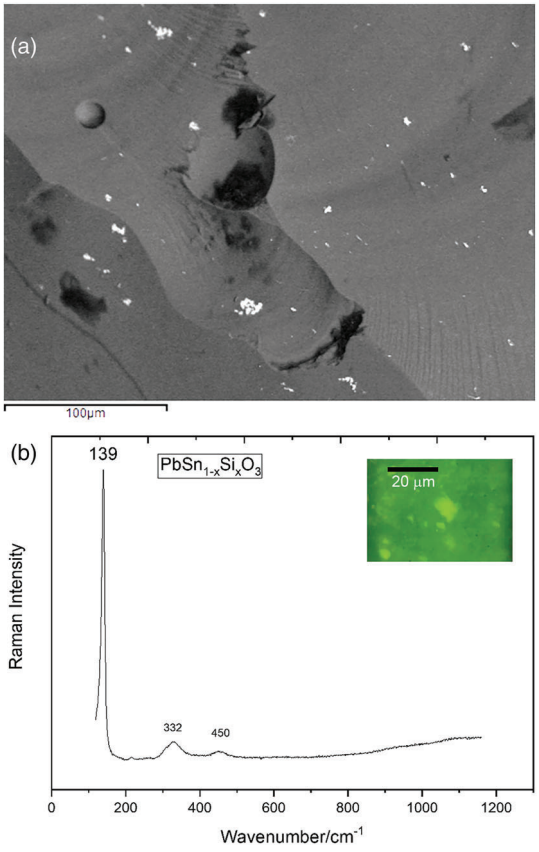

FIGURE 8 Analyses of *tessera* G4. (a) BSE image of $PbSn_{1-x}Si_xO_3$ crystals; (b) microscope image and Raman spectrum of a $PbSn_{1-x}Si_xO_3$ inclusion [Colour figure can be viewed at wileyonlinelibrary.com]

In G2 and G5, in addition to cassiterite, calcium phosphate $Ca_3(PO_4)_2$ acts as opacifier. Its use was indirectly confirmed by the Raman spectrum of some whitish inclusions showing the signature of β-rhenanite (β-$NaCaPO_4$)[23,24] with main peaks at 429, 449, 583, **966**, 1013, 1025, and 1047 cm^{-1} (Figure 9). β-Rhenanite and wollastonite ($CaSiO_3$) are formed when crystals of apatite, belonging to bones used as raw material, react with the glassy matrix at about 700°C.[18] Both phases were identified in G2 and G5. Calcium phosphate (hydroxylapatite), used from fifth to sixth century AD, is the main component of animal bones. They were crushed, powdered, burnt and added to the molten glass to substitute Ca antimonates and tin-based phases, more expensive and less accessible.[23] It is very interesting that this opacifier was identified in blue, turquoise, and green *tesserae* from sites of Eastern Mediterranean, like Turkey, Cyprus, Jordan, Palestine, but also Padua and Ravenna in Italy.[18]

In blue sample B1, FORS technique identified cobalt Co^{2+} as chromophore (minima at 535/595/637 nm) (Figure 10a), in a very low amount, under the detection limit of the used SEM-EDS. The last technique shows the presence of iron (2.1 wt% of Fe_2O_3). Antimony-based opacifiers were employed: they are two calcium antimonate phases, $CaSb_2O_6$ and $CaSb_2O_7$, that coexist in the same sample, with the appearance of crystalline aggregates of white color. The two phases are recognized by their characteristic Raman signals: the spectrum of hexagonal phase ($CaSb_2O_6$) gives peaks at 237, 325, 338, and **670** cm^{-1} (Figure 10b), whereas the spectrum of cubic phase ($CaSb_2O_7$) gives peaks at **480** and **635** cm^{-1} (Figure 10b). The presence of both phases seems to indicate a firing time of 1 or 2 days and a temperature of about 1100°C.[12,18] Sometimes in the Raman spectra, an

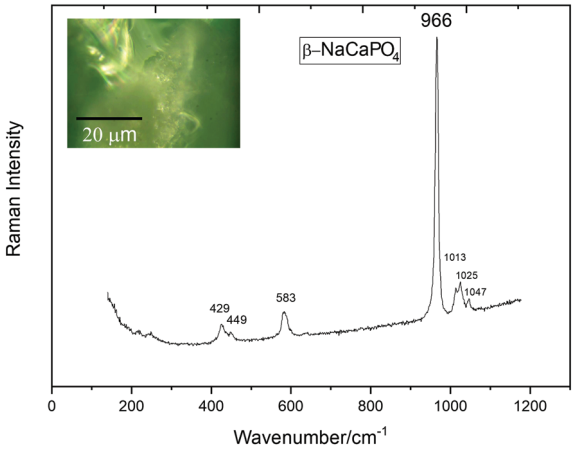

FIGURE 9 Microscope image and Raman spectrum of β-$NaCaPO_4$ crystals in *tessera* G2 [Colour figure can be viewed at wileyonlinelibrary.com]

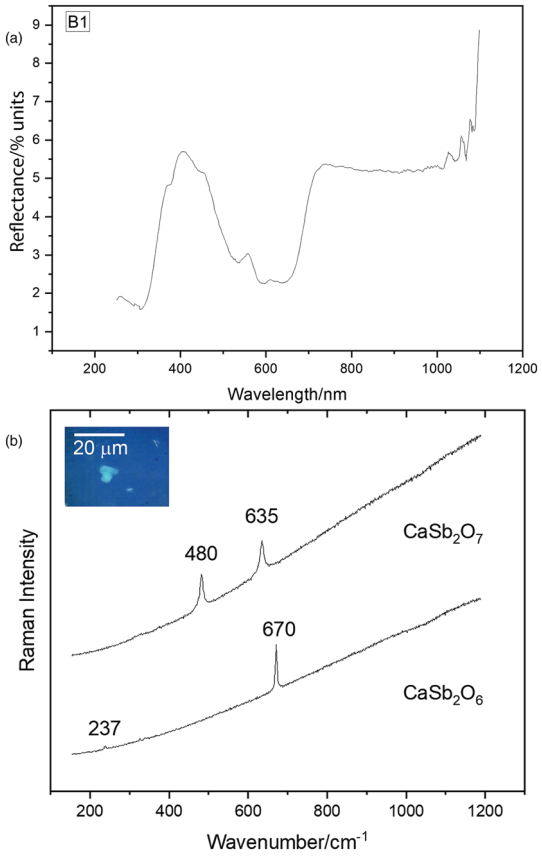

FIGURE 10 Analyses of *tessera* B1. (a) FORS spectrum; (b) Raman spectrum of $CaSb_2O_6$ and $CaSb_2O_7$ and microscope image of calcium antimonate inclusions [Colour figure can be viewed at wileyonlinelibrary.com]

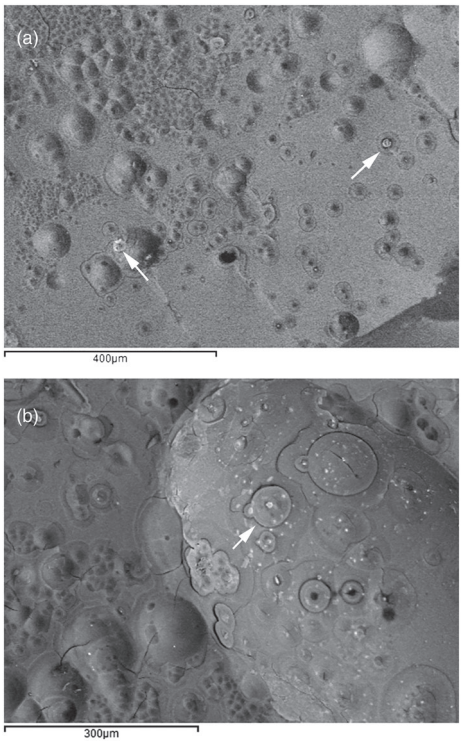

FIGURE 11 BSE images taken on *tessera* B2. (a) Partially fused reaction rims of $Ca_3(PO_4)_2$; (b) partially fused reaction rims of copper

intense peak at 996 cm^{-1} is visible, ascribable to sulfates, perhaps due to remains of raw material used to introduce alkali ions.

For the light blue color of B2, SEM-EDS and FORS recognized copper and iron as colorants; in particular, FORS spectrum shows a minimum at 800 nm (Cu^{2+}) and bands in 375/430 nm (Fe^{3+}), as in G5 (Figure 7b). However, calcium phosphate and cassiterite were employed as opacifiers, identified by means of SEM-EDS and micro-Raman spectroscopy. Regarding calcium phosphate, BSE images highlight partially fused reaction rims (Figure 11a) due to incomplete transformation of hydroxyapatite $Ca_{10}(PO_4)_6(OH)_2$ into β-rhenanite β-$NaCaPO_4$. In the same sample, other reaction rims were caused by incomplete reaction of copper with glass (Figure 11b).

The white hue of W1 is due to two calcium antimonate phases, $CaSb_2O_6$ and $CaSb_2O_7$, acting as both colorants and opacifiers. SEM-EDS data confirm the Raman results, revealing the presence of calcium and antimony in the crystalline inclusions (Figure 12a). As in B1, Raman spectra of sulfates were found (Figure 12b).

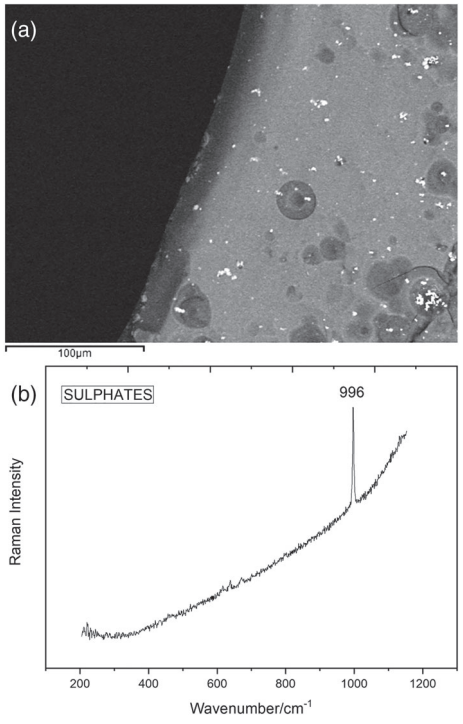

FIGURE 12 Analyses on *tessera* W1. (a) BSE image of aggregates of crystals containing calcium and antimony in W1; (b) Raman spectrum of sulfate inclusions

SEM-EDS demonstrates that black sample was colored by manganese (MnO 3.4 wt%) in combination with iron (Fe_2O_3 12.7 wt%).

The metal leaf *tesserae* are composite materials because they are made of a gold or silver leaf hot fixed among two glass layers: the support (embedded in the mortar) and a thin glass sheet, called *cartellina*, which protects the metal leaf and adds brilliance.[7] In T1 and T2, metal leaf was made of gold (95 wt% T1, 90 wt% T2) and silver (5 wt% T1, 10 wt% T2); in fact, during late antique and Byzantine periods, gold leaves were produced with pure gold or gold–silver alloys.[25]

Comparing the results reported in this work with the data of other studies about glass mosaic *tesserae* of Late Antiquity period,[7,19,23] and in particular with a close context like Ravenna,[26] it appears that the coloring agents are essentially the same, suggesting the presence of a well-established technology in the manufacturing centers of glass tiles. Important differences are instead observed in the opacifiers. Most of them, especially antimonates, are similar in the different contexts, but in the *tesserae* found in *Villa di Teodorico*, there is a diffuse presence of opacifying agents based on tin (cassiterite) and calcium phosphates. This indicates the increasing use of more recent production technologies.

4 | CONCLUSIONS

Archaeometric investigation of glass mosaic *tesserae* of the *Villa di Teodorico* in Galeata was carried out by a multi-technique approach that included the use of micro-Raman spectroscopy, FORS, and SEM-EDS together with XRPD (for only red and orange samples) to obtain essential information about raw materials, composition, and structure of glassy matrix and crystalline inclusions that mainly acted as colorants or/and opacifiers.

This set of samples is made of soda-lime-silica glass, with natron as a flux and calcium and aluminum in variable quantity. In green and red *tesserae*, high levels of lead were found, likely introduced to intensify sparkle of glass, whereas lead is specifically used to produce the orange sample.

Polymerization index obtained by Raman spectra and composition of opacifiers suggest a processing temperature of about 1000°C, maximum temperature reachable by ancient furnaces.

Color and opacity of glass is due to chromophore ions and/or opacifying/coloring crystals. Black hue was obtained by manganese and iron. Calcium antimonates ($CaSb_2O_6$ and $CaSb_2O_7$) were employed in white and cobalt-colored blue glasses, whereas pink shade was obtained by lead antimonates ($Pb_2Sb_2O_7$) with manganese and iron ions. Lead–tin yellow type II ($PbSn_{1-x}Si_xO_3$) and cassiterite (SnO_2) or calcium phosphate $Ca_3(PO_4)_2$ and cassiterite were used with copper and iron ions in green color. Calcium phosphate also was employed in copper and iron-colored light blue glass, whereas cassiterite was also used in red and orange *tesserae*, respectively, colored by metallic copper and cuprite. Antimony-based opacifiers were common during imperial age, but lead–tin yellow type II, cassiterite, and calcium phosphate were attested from Late Antiquity.

Gold leaf *tesserae* are colorless decolorized by manganese, and gold leaves are made with a gold–silver alloy.

These results prove the high technological level reached by specialized manufacturing centers. Moreover, the comparison with other late antique contexts, in particular Ravenna, demonstrates that the chromophores employed are similar, whereas, regarding the opacifiers, in Galeata, there is a more important use of tin and calcium phosphate-based phases, namely, more recent production technologies.

ACKNOWLEDGEMENTS

The archeological excavations were supported, inside S.F.E.R.A. Program and Framework Agreement between Università di Parma and Comune di Galeata, by Archeological Mission at *Villa di Teodorico* in Galeata, led by Università di Parma (director Alessia Morigi, scientific managers Alessia Morigi and Riccardo Villicich) in MiBACT concession.

ORCID

Danilo Bersani https://orcid.org/0000-0002-8026-983X
Luciana Mantovani https://orcid.org/0000-0001-7438-1887
Maurizio Aceto https://orcid.org/0000-0001-6360-3632
Laura Fornasini https://orcid.org/0000-0002-6794-0828

REFERENCES

[1] R. Villicich, A. Morigi, E. Rinaldi, *Archeologia e Calcolatori* **2019**, *30*, 183.
[2] L. Saviane, Gli ambienti ottagonali della villa di Teodorico a Galeata e nell'architettura residenziale tardoantica, Degree Thesis, Università di Parma (Italy), **2017**/2018.
[3] A. Morigi, R. Villicich, *FOLD&R. J. Fasti Online* **2020**, 466.
[4] P. Ricciardi, P. Colomban, A. Tournié, M. Macchiarola, N. Ayed, *J. Archaeol. Sci.* **2009**, *36*, 2551.
[5] E. Basso, C. Invernizzi, M. Malagodi, M. F. La Russa, D. Bersani, P. P. Lottici, *J. Raman Spectrosc.* **2014**, *45*, 238.
[6] A. Rousaki, M. Costa, D. Saelens, S. Lycke, A. Sánchez, J. Tuñón, B. Ceprián, P. Amate, M. Montejo, J. Mirão, P. Vandenabeele, *J. Raman Spectrosc.* **2020**, *51*, 1913.
[7] A. Conventi, E. Neri, M. Verità, *Mater. Sci. Eng. A* **2012**, *32*, 012007.
[8] D. Barca, E. Basso, D. Bersani, G. Galli, C. Invernizzi, M. F. La Russa, P. P. Lottici, M. Malagodi, S. A. Ruffolo, *Microchem. J.* **2016**, *124*, 726.

[9] N. Schibille, C. Boschetti, M. A. Valero Tévar, E. Veron, J. De Juan Ares, *Minerals* **2020**, *10*, 272.
[10] M. Aceto, G. Fenoglio, M. Labate, M. Picollo, M. Bacci, A. Agostino, *Journal of Cultural Heritage* **2020**, *45*, 33.
[11] M. Bandiera, M. Verità, P. Lehuédé, M. Vilarigues, *Minerals* **2020**, *10*, 875.
[12] S. Maltoni, A. Silvestri, *Minerals* **2018**, *8*, 255.
[13] C. M. Jackson, *Archaeometry* **2005**, *47*, 763.
[14] P. Colomban, M. P. Etcheverry, M. Asquier, M. Bounichou, A. Tournié, *J. Raman Spectrosc.* **2006**, *37*, 614.
[15] P. Colomban, A. Tournié, L. Bellot-Gurlet, *J. Raman Spectrosc.* **2006**, *37*, 841.
[16] P. Colomban, *J. Non Cryst. Solids* **2003**, *323*, 180.
[17] P. Colomban, *J. Cult. Herit.* **2008**, *9*, e55.
[18] M. Vandini, S. Fiorentino, *Minerals* **2020**, *10*, 609.
[19] E. Neri, C. Morvan, P. Colomban, M. F. Guerra, V. Prigent, *Ceram. Int.* **2016**, *42*, 18859.
[20] M. Tite, T. Pradell, A. Shortland, *Archaeometry* **2008**, *50*, 67.
[21] S. Lahlil, M. Cotte, I. Biron, J. Szlachetko, N. Menguy, J. Susini, *J. Anal. At. Spectrom* **2011**, *26*, 1040.
[22] S. Galli, M. Mastelloni, R. Ponterio, G. Sabatino, M. Triscari, *J. Raman Spectrosc.* **2004**, *35*, 622.
[23] A. Silvestri, F. Nestola, L. Peruzzo, *Microchem. J.* **2016**, *124*, 811.
[24] W. Suchanek, M. Yashima, M. Kakihana, M. Yoshimura, *J. Eur. Ceram. Soc.* **1998**, *18*, 1923.
[25] E. Neri, M. Verità, *J. Archaeol. Sci.* **2013**, *40*, 4596.
[26] S. Fiorentino, T. Chinni, M. Vandini, *J. Cult. Herit.* **2020**, *46*, 335.

How to cite this article: D. Bersani, L. Saviane, A. Morigi, L. Mantovani, M. Aceto, L. Fornasini, *J Raman Spectrosc* **2021**, 1. https://doi.org/10.1002/jrs.6180